Journal of The Korean Astronomical Society
37: 361 ∼ 369, 2004

X-RAY STUDIES OF THE INTRACLUSTER MEDIUM IN CLUSTERS OF GALAXIES - CHARACTERIZING GALAXY CLUSTERS AS GIANT LABORATORIES

Hans Böhringer
Max-Planck-Institut für extraterrestrische Physik, D-85748 Garching, Germany
E-mail: hxb@mpe.mpg.de

ABSTRACT

Galaxy clusters as the densest and most prominent regions within the large-scale structure can be used as well characterizable laboratories to study astrophysical processes on the largest scales. X-ray observations provide currently the best way to determine the physical properties of galaxy clusters and the environmental parameters that describe them as laboratories. We illustrate this use of galaxy clusters and the precision of our understanding of them as laboratory environments with several examples. Their application to determine the matter composition of the Universe shows good agreement with results from other methods and is therefore a good test of our understanding. We test the reliability of mass measurements and illustrate the use of X-ray diagnostics to study the dynamical state of clusters. We discuss further studies on turbulence in the cluster ICM, the interaction of central AGN with the radiatively cooling plasma in cluster cooling cores and the lessons learned from the ICM enrichment by heavy elements.

Key words : clusters of galaxies – cosmology – intergalactic medium

I. INTRODUCTION

Galaxy clusters are the largest well defined objects in the hierarchy of structures in the Universe. In contrast to their name, which characterizes them rather as collections of objects, they show up as unit entities in X-rays, as shown in Fig. 1. They have been formed from the densest regions in the large-scale matter distribution of the Universe at scales of the order of 10 Mpc and have collapsed to form matter aggregates that have reached an approximate dynamical equilibrium. They are best seen as large gravitational potentials holding mostly dark matter, hot thermal plasma, and galaxies together, roughly in proportions of 87%, 11%, and 2%, respectively. Here an throughout the paper we adopt a Hubble constant of $H_0 = 70$ km s^{-1} Mpc^{-1} if not stated otherwise.

Thus galaxy clusters are the largest objects in the Universe which have a characteristic form, which can be well assessed by observations and well described by theoretical modeling. With these properties they also form the largest astrophysical laboratories, in which the physical environmental conditions can be well observed and described. As the most prominent regions in the large-scale structure distribution of the Universe they form therefore perfect laboratory sites for detailed studies of the processes which are the topic of this conference, magnetic fields and cosmic particle generation, on the largest scales.

The aim of this contribution is therefore to give an overview on how well we currently understand these galaxy cluster laboratories, by providing a background of the observational characterization of clusters and by illustrating the degree of our understanding by some prime examples which partly also relate to the topic of this meeting.

Fig. 1.— The Coma cluster of galaxies as seen in X-rays in the ROSAT All-Sky Survey (underlaying red color) and the optically visible galaxy distribution in the Palomar Sky Survey Image (galaxy and stellar images from the digitized POSS plate superposed).

Proceedings of The 3rd Korean Astrophysics Workshop on *Cosmic Rays and Magnetic Fields in Large Scale Structure*

As mentioned above, X-ray observations play currently a prime role in the observational studies of the structure and astrophysics of clusters of galaxies. This is due to the hot intracluster medium (ICM), a hot thermal plasma that fills the whole cluster volume, has temperatures in the range of 10 to 100 Million Kelvin, and emits the maximum of its thermal radiation in the soft X-ray band - just the energy range in which we can build and operate imaging X-ray telescopes. Galaxy clusters are therefore among the most rewarding objects for X-ray imaging studies next to supernova remnants. Since the X-ray emission is proportional to the squared plasma density, the ICM density can be reconstructed from the observed X-ray images if we make some presumptions on the three-dimensional geometry of the clusters that allows us the deprojection of the surface brightness distribution. Also the temperature of the ICM can be determined by X-ray spectroscopy. The thermal emission leads to optically thin radiation in which every electron-ion collision leads to an emitted photon. The spectral form is independent from the normalization only dependent on the temperature and chemical composition of the plasma and both pieces of information can be reliably determined from the spectral appearance. The only remaining ambiguities are again that the observed spectrum is a projection of thermal emission along the line of sight and the existence of a range of different temperatures can not easily and unambiguously unfolded. Thus we observe what is often called an "emission measure weighted temperature" and further assumptions play a role in the unfolding and deprojection of the measurement. However, the best observed spectra, e.g. in the X-ray halo of M87 (Matsushita et al. 2002) provide good support for an uncomplicated scenario with a good approximation of ionization equilibrium, local isothermality, and smooth temperature variations as a function of radius, which allows us a good assessment of the structure of the ICM. The knowledge of the density and temperature structure also yields information on the pressure and entropy distribution. And if we can assume approximate pressure equilibrium - an assumption that we also discuss later - we can use the pressure distribution in the ICM to infer the structure of the gravitational potential and the mass distribution of the cluster.

II. MATTER COMPOSITION OF GALAXY CLUSTERS

The new X-ray satellite observatories XMM-Newton (ESA) and CHANDRA (NASA) now provide advanced observational capabilities to derive spatially resolved spectroscopic information that allows us to reconstruct the density and temperature distribution of the ICM in the way described above. The CHANDRA observatory provides a superior angular resolution of less than one arcsec showing many important details in the ICM distribution like cold fronts (Vikhlinin et al. 2002), shock waves (Markevitch et al. 2002), and X-ray cavities blown by AGN radio lobes (Böhringer et al. 1993, Fabian et al. 2003). The large X-ray collecting power of XMM-Newton provides good photon statistics that allows to construct X-ray spectra from different regions and features seen in the X-ray images giving a good overview on the temperature structure of the clusters. In addition the highly sensitive reflection grating instruments, RGS, on board of XMM have given us the most detailed line spectra of the cluster ICM. It is also with XMM-Newton that we get the best information on the low surface brightness region in the outer parts of the clusters.

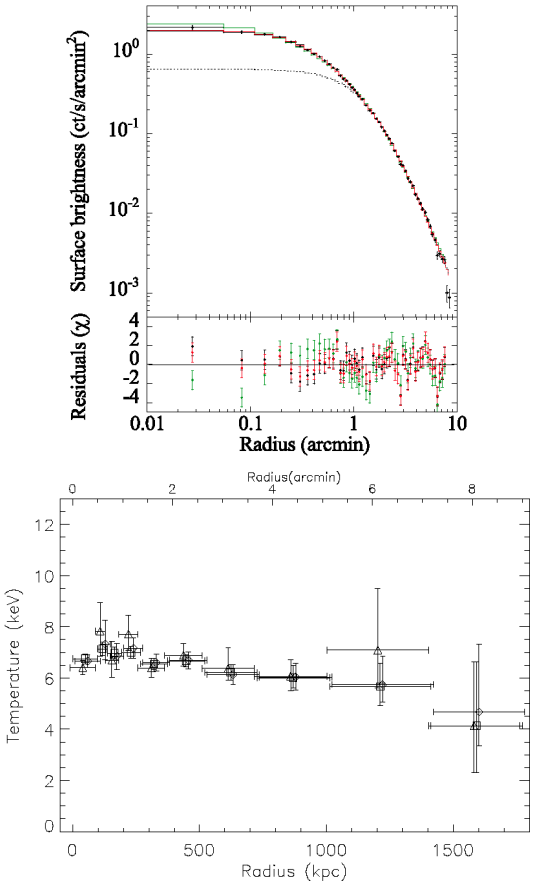

Fig. 2.— Upper panel: Surface brightness profile of the galaxy cluster Abell 1413 determined from an XMM-Newton observation by Pratt & Arnaud (2002). **Lower panel:** Temperature profile of the ICM of the galaxy cluster Abell 1413 from an XMM-Newton observation by Pratt & Arnaud (2002). The temperature profile extends to a radius of about r_{500}.

Fig. 2 gives an example of one of the best X-ray studies of a galaxy cluster with XMM-Newton so far, of Abell 1413 (Pratt & Arnaud 2002). The figure shows the accuracy of the determination of the cluster surface brightness profile and the temperature profile. The temperature profile extends to about a radius of an overdensity of 500 over the critical density of the Uni-

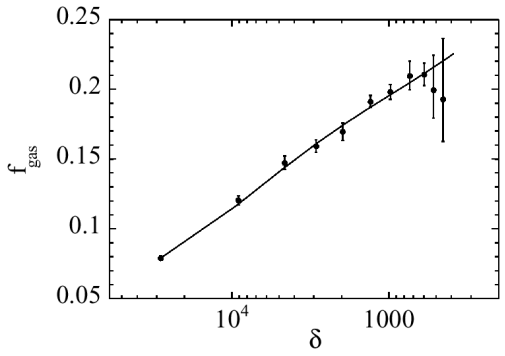

Fig. 3.— ICM gas mass fraction in the galaxy cluster Abell 1413 from an XMM-Newton observation by Pratt & Arnaud (2002).

verse, r_{500}, which is about 60% of the radius of the dynamical edge of the virialized galaxy cluster (e.g. Evrard 1997, Voit 2004). From these data the gravitational mass and gas mass profile can be determined. The ratio of the two gives the gas mass fraction. The result for the gas mass fraction profile for this cluster is shown in Fig. 3. In the outer region the gas mass fraction is asymptotically approaching a value of about $11\% h_{70}^{3/2}$ (note that the results in the figure are given for a Hubble constant of $h_{50} = H_0/(50\mathrm{kms}^{-1}\mathrm{Mpc}^{-1}) = 1$). Together with the stellar mass in the cluster galaxies of about 2% this mass of about 13% is believed to account for the vast majority of the baryonic mass in the galaxy cluster. The rest of the mass, the so called "missing mass" since the time of Zwicky (1937), is attributed to dark matter. Other studies of the cluster baryon fraction based on CHANDRA observations by Allen et al. (2003, 2004) and Ettori et al. (2003) and earlier determinations with less precise data (Briel et al. 1991, Böhringer et al. 1993, Evrard 1997, Mohr et al. 1999, Ettori & Fabian 1999, Ettori et al. 2001) yield very similar results.

Since galaxy clusters are formed essentially by gravitational collapse which samples all forms of matter almost indiscriminently into the cluster potential, this ratio should give a measure of the ratio of baryons to dark matter of the Universe. This cosmic ratio has also been measured by other means, like the fluctuation spectrum of the cosmic microwave background (e.g. Spergel et al. 2003) or the primordial deuterium abundance in connection with nucleosythesis calculations (Burles et al. 2001) with results summarized in Table 1. There is good agreement within the quoted error limits of about 10% among all three methods. This provides good support for the reliability of the mass and gas mass determination in galaxy clusters.

Table 1. Baryon mass density fraction in the Universe determined by different methods: galaxy cluster composition, nucleosynthesis combined with the observed primordial deuterium abundance, and the relative heights of the peaks in the cosmic microwave background fluctuation power spectrum (from WAMP).

method	$\Omega_b\ h^2$	Ω_b for $h = 0.7$
cluster baryon fraction (assuming that nucleosynthesis & primordial deuterium	$\Omega_m = 0.3$)	0.0390
	0.0205($\pm$0.0019)	0.0407
WMAP CMB fluct. spectrum	0.0224($\pm$0.0009)	0.0444

III. EXPLORATION OF CLUSTER STRUCTURE

(a) Mass Determination

Fig. 4 shows the mass profile determined from the same data as above (Pratt & Arnaud 2002). The mass profile can be reasonably well fit by a NFW mass profile (Navarro et al. 1996). This has also been found in a series of detailed inspections of mass profiles from XMM-Newton and CHANDRA (e.g. Allen et al., 2003 Buote & Lewis 2004), with the conclusion that most well relaxed appearing clusters follow this description, but clusters showing some distortion, most probably due to recent merger activity, have cores which are too flat to be described by NFW profiles (e.g. Pratt et al. 2004).

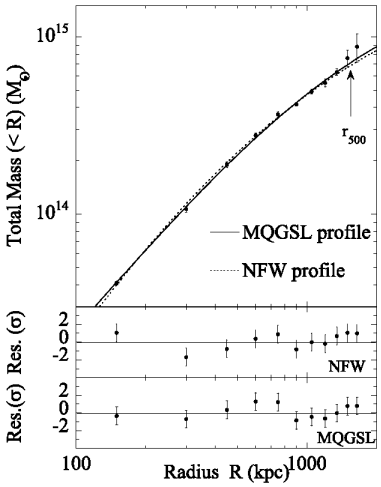

Fig. 4.— Mass profile of the cluster Abell 1413 determined from XMM-Newton observations by Pratt & Arnaud (2002). The figure illustrates how well the profile can be fitted by the proposed, theoretically derived mass models by Navarro et al. (1996) and Moore et al. (1999).

One of the urgent questions is of course how reliable the determined masses are. The answer to this question has far reaching consequences for several cosmological applications of galaxy clusters as for example the use of the baryon fraction for cosmological tests, but also for the use of galaxy clusters to assess the cosmic large-scale structure in the matter distribution (e.g. Collins

et al. 2000, Schuecker et al. 2001, 2002, Böhringer et al. 2002a). Like the baryon fraction studies also the latter cosmological application has given us some confidence in the determined cluster masses.

(b) Comparison to Lensing Studies

One possibility to test the mass measurement with an independent method is the comparison to the gravitational lensing effect of clusters. The more massive and compact galaxy clusters reach the critical projected mass density in the center necessary for the strong gravitational lensing effect, which gives rise to spectacular arcs (e.g. Mellier 1999), but all clusters are expected to show weak gravitational shear. It has been pointed out in a series of publications, that the masses inferred from gravitational lensing tend to be larger than those determined from X-ray observations (e.g. Wu 2000). Magnetic fields and cosmic rays producing an additional ICM pressure were among the effects proposed to overcome this discrepancy (Loeb & Mao 1995) which seems worth mentioning within the context of the present conference.

We have studied a series of famous lensing clusters with new X-ray observations. A first example is Abell 2390, which has a very compact and symmetric appearance with a slight ellipticity and a very prominent cooling core. The cluster has a prominent tangential and radial arc (Pierre et al. 1996) and shows a well detected weak lensing effect on large scale (Squires et al. 1996). The cluster has also been subject of very detailed spectroscopic studies in the optical by Carlberg et al. (1996) from which a mass profile was determined from the galaxy dynamics. Combined deep X-ray studies with ROSAT and ASCA provide a good X-ray mass measurement (Böhringer et al. 1998) which was later also exactly confirmed with CHANDRA data (Allen et al. 2001). A comparison of all these mass profile results given in Fig 5 shows that there is excellent agreement.

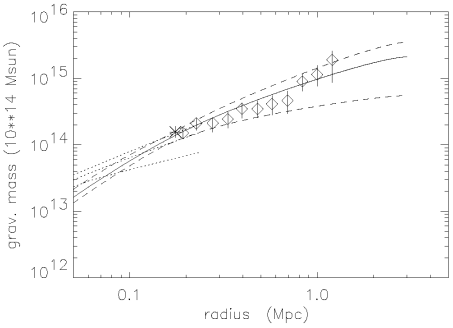

Fig. 5.— Radial mass profile of A2390 determined from X-ray data (lines, Böhringer et al. 1998), strong lensing (asterisk, Pierre et al. 1996) and Weak lensing (diamonds, Squires et al. 1996).

Further prominent lensing clusters for which no good agreement has been obtained comprise for example Abell 2218, Abell 1689 and CL0024+17. Fig. 6 shows a comparison of the X-ray and lensing result for CL0024+17 (Zhang et al. 2004a, Soucail et al. 2000, Böhringer et al. 2000). The X-ray image of this cluster shows some complex asymmetric features in the cluster core region, but gives no direct clue on the reason for these disturbances. The explanation comes from the study of the galaxy velocity distribution in these clusters (Czoske et al. 2002), which clearly indicates that the cluster is a configuration where two major subclusters are merging in the direction very close to the line-of-sight.

The cases of Abell 1689 (King et al. 2002, Czoske 2003) and Abell 2218 (Pratt et al. 2004, Girardi et al. 1997) turn out to be similar line-of-sight mergers. Such well oriented configurations captured in the special moment of collapse should be rare, and thus should not concern the mass determination in the average cluster. But due to the extra mass in the filament projected onto the cluster surface in the line-of-sight, they appear as such spectacular lensed objects and have preferentially been selected as lensing study targets. Thus the discrepancies in the determined masses is not a defect in the method, but very different masses are assessed. While the X-ray mass measurement provides a result on the mass of the collapsed and partly relaxed core of the clusters, the lensing measurement provides an account of the matter filament in which the cluster is embedded.

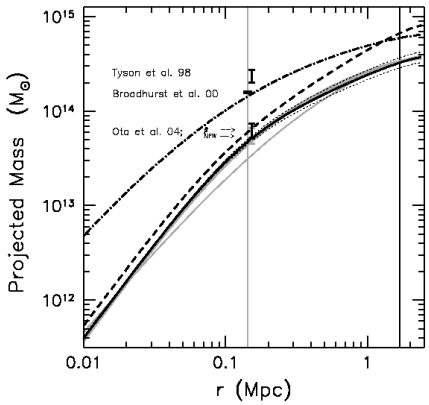

Fig. 6.— Projected mass profile of the cluster CL0024+17 (thick line) from XMM-Newton observations compared to strong gravitational lensing results (Zhang et al. 2004a).

(c) Self-Similarity of Cluster Structure and Structure Diagnostics

The examples of well relaxed and merging clusters encountered in the last subsection show that galaxy clusters come with a variety of shapes. In this context it is important to know how much self-similarity there is between clusters as a function of mass. After all, the formation of galaxy clusters through gravitational collapse is a self-similar processes in which only the substructure in the initial conditions introduces some smaller differences. A knowledge of the cluster self-similarity and its scatter allows us to predict within

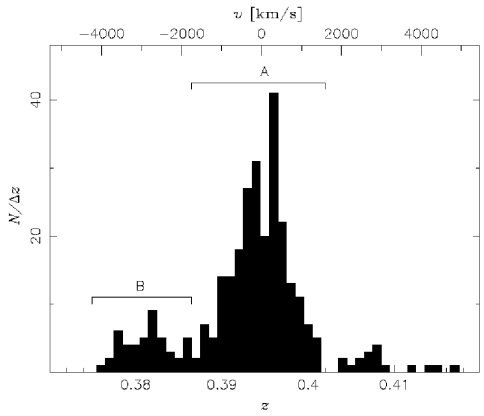

Fig. 7.— Redshift distribution of the galaxies in the cluster CL0024+17 from Czoske et al. (2002)

certain limits cluster properties from one or a few observables (e.g. to get a mass estimate from an X-ray luminosity).

Fig. 8 shows for example a set of surface brightness and temperature profiles for a statistical sample of massive galaxy clusters at redshifts around $z \sim 3$ from the ROSAT All-Sky Survey (Zhang et al. 2004b). The temperature structure and the gas density profiles are pretty similar, with the largest diversity in the central regions where we can distinguish cooling core and non-cooling core clusters.

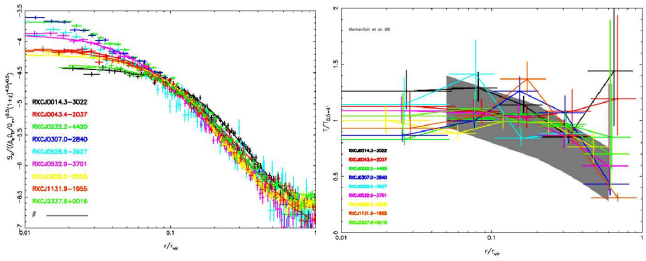

Fig. 8.— Surface brightness and temperature profiles of X-ray luminous REFLEX clusters (REFLEX-DXL, Zhang et al. 2004b) which illustrate the large degree of self-similarity of galaxy clusters. The profiles are scaled by the estimated virial radius and the temperature axis on the right panel by the bulk temperature. The grey region shows the temperature profiles from Markevitch's (1998) ASCA analysis.

As a further diagnostics of the cluster structure the spectral imaging capabilities of XMM and CHANDRA allow us to produce projected temperature, density, pressure and entropy maps. While the entropy map provides a good insight into the history of cluster formation, the pressure map is diagnostics of disturbances of the hydrostatic equilibrium. Fig. 9 provides a particularly interesting example of a high speed merger where a small subclump is shot through the main cluster and is preceded by a bow shock, seen as bright feature in the entropy map in the NW of the cluster (Finoguenov et al. in preparation). The lesson learned from the study of a series of such diagnostic maps is that the pressure maps usually appear quite regular (as in the present case where it is the most symmetric map) which supports the assumption of approximate hydrostatic equilibrium in the cluster mass determination.

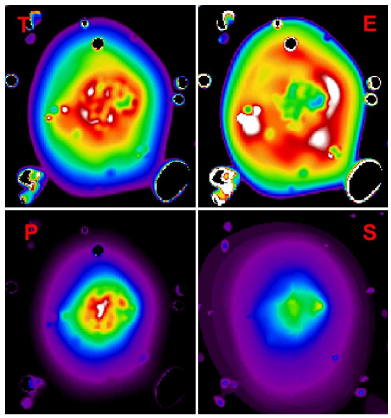

Fig. 9.— Temperature (T), entropy (E), pressure (P) and surface brightness (S) map of the cluster RXCJ0658-5557 (Finoguenov et al. in preparation) constructed from XMM-Newton imaging and spectroscopic data.

IV. PROBING TURBULENCE IN THE CLUSTER ICM

One of the open questions concerning the structure of the ICM is how much pressure and kinetic energy content is present in the form irregular gas motions and turbulence. The main driver for turbulence is the enormous amount of energy released in cluster mergers and turbulence is one possible driver for the generation of cosmic rays. A detailed XMM-Newton X-ray observation of the Coma Cluster, which is believed to be in a post-merger stage, has now given us a first clue on the observation of turbulence (Schuecker et al. 2004). The most direct description of turbulence is of course through the velocity field. A consequence of the random velocities are pressure fluctuations which can be traced in the pressure maps that can be constructed from the observed surface brightness and temperature distribution of the X-ray emitting plasma (Fig. 10).

For turbulence we expect to see three characteristic features in the pressure, temperature and density distribution of the ICM. For developed turbulence the pressure fluctuations should be Gaussian, which is shown for the Coma ICM in Fig. 11 For subsonic turbulence the density and temperature fluctuations should follow the equation $\Delta T/T = (\Delta n^2/n^2)^{4/3}$ which is approximately fulfilled as shown in Fig... Finally the three-dimensional Fourrier spectrum of the fluctuations should follow a power law $\Delta P \propto k^{-7/3}$ given by the theory of Kolmogorov (1941) and Oboukhov (1941). Fig. 13 shows that such a power law is actually observed (in projection) in Coma for scales from 2.8 Mpc down to about 20 kpc (for details see Schuecker et al. 2004). Other signatures of turbulence in the cluster ICM have been found and discussed by Inogamov & Sunyaev (2003) and Vogt & Enßlin (2003).

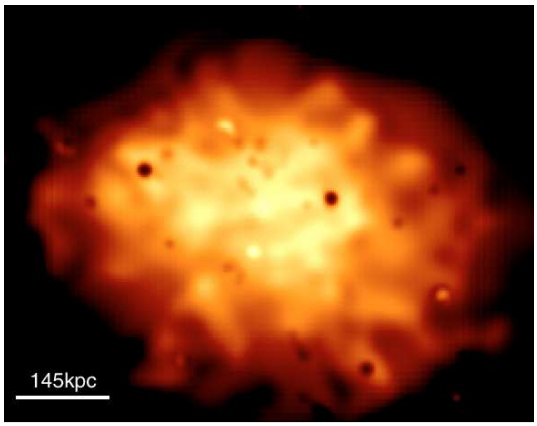

Fig. 10.— Image of the projected pressure distribution of the Coma cluster (Schuecker et al. 2004). The scale of 145 kpc corresponds to the largest size of turbulent eddies indicated by the power spectrum.

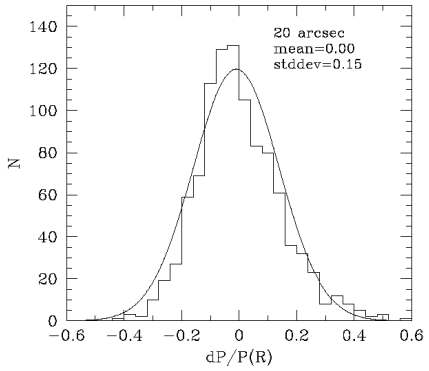

Fig. 11.— Histogram of the pressure fluctuations with an approximate Gaussian shape.

V. COOLING AND HEATING OF THE ICM AND AGN-ICM INTERACTION

X-ray observations of galaxy clusters more than 25 years ago showed that the cooling time in the central ICM of some clusters is shorter than the Hubble time. The most direct conclusion is that the hot plasma in the central region is cooling and condensing, causing an influx of gas from the outer regions, the scenario of cooling flows (Fabian & Nulsen 1977). The reheating of the gas seemed implausible since the heating source has to be fine tuned not to disperse the gas and to provide enough energy input to counteract the radiative cooling (Fabian 1994). New observations with XMM-Newton and CHANDRA lead to a revision of this scenario. The high resolution CHANDRA images now show various examples of interaction effects of central AGN with the cluster ICM providing direct evidence of energy input into the radiatively cooling ICM (e.g. McNamara et al. 2000, Birzan et al. 2004, Forman et al. 2004) as shown in Fig 14 (Fabian et al. 2003). The high resolution spectroscopy with the RGS instruments (e.g. Peterson et al. 2001) and the spatially resolved spectroscopy of the EPIC cameras (e.g. Matsushita et al.

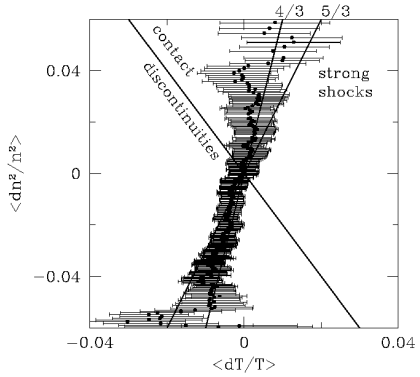

Fig. 12.— Correlation of the density and temperature fluctuations with an approximately adiabatic signature.

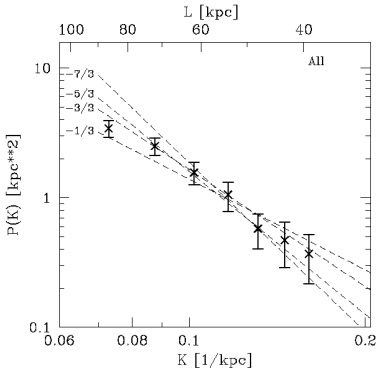

Fig. 13.— Power spectrum of the pressure fluctuations in the turbulent ICM of the Coma cluster (Schuecker et al. 2004).

2002) on board of XMM-Newton showed that a continuous coverage of the temperature range down to low temperatures as expected for continued cooling of the central ICM is not observed in the spectra. These two new pieces of information have lead to the new emerging picture of cluster cooling cores, where the fine tuned reheating of the cooling central ICM is achieved by the cycle of feeding a central AGN with cooling flow gas until the energy output of the AGN is limiting (regulating) the further cooling of the ICM, such that the gas condensation rates are reduced by factors of probably tens to hundreds (e.g. Churazov et al. 2000, 2001, Böhringer et al. 2002).

VI. HEAVY ELEMENT ABUNDANCE DIAGNOSTICS

The central ICM of cooling core clusters is also characterized by a central heavy element abundance peak (Fig. 15: see also De Grandi & Molendi 2001) which provides interesting insights into the heavy element production and further diagnostics of the history of the cooling core regions. We know two sources for the enrichment of the ICM with heavy elements: core collapse supernovae, type II, which produce a broad spectrum of element masses with a bias towards the lighter elements

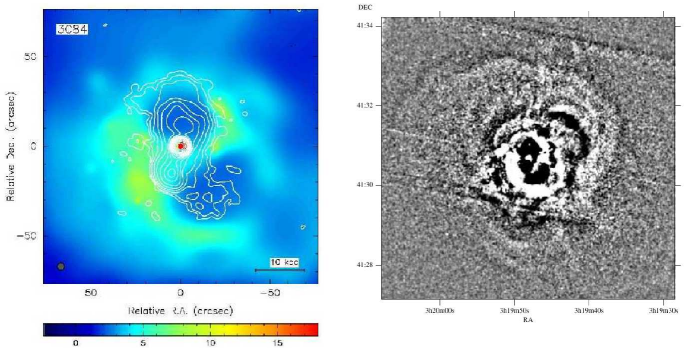

Fig. 14.— Interaction of the AGN in NGC1275 with the ICM of the Perseus cluster observed with CHANDRA (Fabian et al. 2003). The left picture shows the X-ray emission with the radio image as contour lines. We see that the radio lobe plasma has displaced the thermal gas. The right picture is an unsharp masked image of the X-ray emission showing "ripples" caused by the AGN energy input into the ICM.

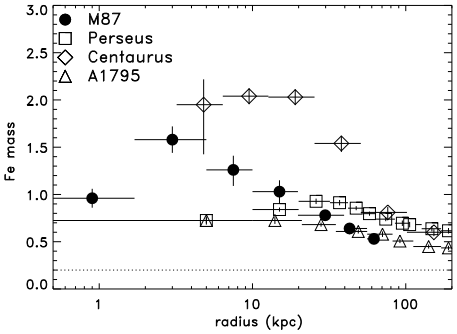

Fig. 15.— Relative abundance distribution of Fe in the ICM of four nearby clusters as deduced from XMM-Newton observations (Böhringer et al. 2004).

like O and Mg, and type Ia supernovae, thermonuclear explosions of white dwarfs, which dominantly yield Fe group elements and lighter elements like Si and S but very little O and Mg. A close inspection of the composition of the central abundance peak shows that it is traced by the heavier SN Ia products but not by the lighter elements like O and Mg (Fig. 16, Matsushita et al. 2003). This is consistent with the picture that SN II activity happens in the early history of cluster formation when the stellar populations of the cluster galaxies are still young and SN II products become well mixed. SN Ia are still observed in the present day cluster ellipticals. The more recent yields obviously lead to more local enrichment, in particular the massive stellar population of the cD galaxies dominating the centers of cooling core clusters are responsible for the central enrichment.

(a) Enrichment Times

The central abundance peak extends much further than the central 10 kpc region inside the central galaxy. Since the central galaxy dominates the stellar population out to radii of the order of 100 kpc and is therefore responsible for most of the secular heavy elements in

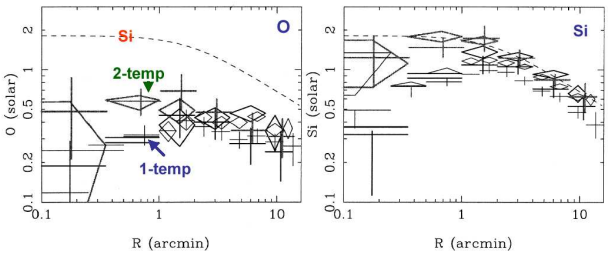

Fig. 16.— Abundance profiles of O and Si in the X-ray halo of M87 in the Virgo cluster as deduced from XMM-Newton observations (Matsushita et al. 2003).

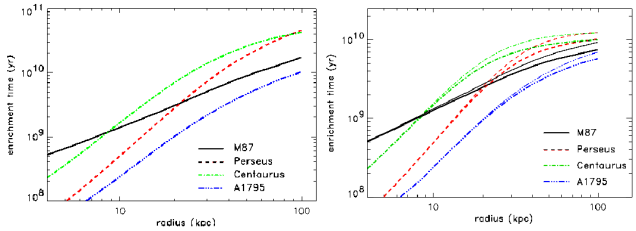

Fig. 17.— Enrichment ages of the central iron abundance peak in the four galaxy clusters, M87/Virgo, Centaurus, Perseus, and A1795. The enrichment times were calculated on the basis of a SN Ia rate of 0.15 SNU (Capellaro et al. 1999) and an additional contribution by stellar mass loss. **Left panel:** with constant SN Ia rate, **Right panel:** with increasing SN Ia rate in the past described by a power law with time exponents $s = -2$ (thick lines) and $s = -1.1$. (thin lines).

this zone, this implies some transport of the centrally enriched ICM to larger radii and large enrichment times to produce all the iron in the entire abundance peak. With an Fe production with a supernova rate of 0.15 SNU (Cappelaro et al. 1999) and stellar mass loss rates of $2.5 \cdot 10^{-11} \times L_B$ (Ciotti et al. 1991) we can calculate the enrichment times of the Fe in the abundance peak as a function of radius, with results shown in Fig. 17. In a second, alternative model the SN Ia rate is assumed to be larger in the past. Even for the second model we find quite large enrichment times of $5-9$ Gyrs for radii around 50 kpc and 7 to 12 Gyrs for 100 kpc. If the estimates are correct these results imply that the central regions of the clusters and their ICM can not have suffered major disturbances during these times and that the ICM experiences only mild turbulent redistribution. The central regions of cooling flow clusters must therefore be rather old. This scenario would not allow the inclusion of cooling flows with the large previously inferred mass deposition rates, since this would make the accumulation of the large observed central excess Fe masses of the order of 10^9 $M_\odot$ impossible.

VII. CONCLUSION

The broad range of topics described illustrate the rich knowledge gained on galaxy clusters as astrophysical laboratories with a large, very recent progress thanks to the X-ray observatories CHANDRA and XMM-Newton.

ACKNOWLEDGEMENTS

I like to thank Prof. Dongsu Ryu and Prof. Hyesung Kang very much for organizing this wonderful conference and also for introducing us with so much warmth and welcome to Korean culture.

A major part of this work was achieved with X-ray observations using the satellite X-ray observatory XMM-Newton , an ESA mission with instruments and contributions directly funded by ESA member States and the USA (NASA). The XMM-Newton Project is supported by the Bundesministerium für Bildung und Forschung, the Max-Planck-Society, and the Haidenhain Stiftung.

REFERENCES

Allen, S. W., Ettori, S., Fabian, A. C., 2001, MNRAS 324, 877

Allen, S. W., Schmidt, R. W., Fabian, A. C., Ebeling, H., 2003, MNRAS, 342, 287

Allen, S. W., Schmidt, R. W., Ebeling, H., Fabian, A. C., van Speybroeck, L., 2004, MNRAS, 353, 457

Birzan, L., Rafferty, D. A., McNamara, B. R., Wise, M. W., Nulsen, P. E. J., 2004, ApJ, 607, 800

Böhringer, H., Voges, W., Fabian, A. C., Edge, A. C., Neumann, D. M., 1993, MNRAS, 264, L25

Böhringer, H., Tanaka, Y., Mushotzky, R. F., Ikebe, Y., Hattori, M., 1998, A&A, 334, 789

Böhringer, H., Collins, C. A., Guzzo, L., Schuecker, P., et al. 2002, ApJ, 566, 93

Böhringer, Matsushita, K., Churazov, E., Ikebe, Y., Chen, Y., 2002b, A&A, 382, 804

Böhringer, H., Matsushita, K., Churazov, E., Finoguenov, A., Ikebe, Y., 2004, A&A, 416, 21

Buote, D. A., Lewis, A. D., 2004, ApJ, 604, 116

Burles, S., Nollet, K. M., Turner, M. S., 2001, ApJ, 552, L1

Cappellaro, E., Evans, R., Turatto, M., 1999, A&A, 351, 459

Carlberg, R. G., Yee, H. K. C., Ellingson, E., Abraham, R., Gravel, P., Morris, S., Pritchet, C. J., 1996, ApJ, 462, 32

Churazov, E., Forman, W., Jones, C., Böhringer, H., 2000, A&A, 356, 788

Churazov, E., Brüggen, M., Kaiser, C. R., Böhringer, H., Forman, W., 2001, ApJ, 554, 261

Ciotti, L., Pellegrini, S., Renzini, A., D'Ercole, A., 1991, ApJ, 376, 380

Collins, C. A., Guzzo, L., Böhringer, H., Schuecker, P., 2000, MNRAS, 319, 939

Czoske, O., Moore, B., Kneib, J.-P., Soucail, G., 2002, A&A, 368,31

De Grandi, S., Molendi, S., 2001, ApJ, 551, 153

Ettori, S., 2001, MNRAS, 323, L1

Ettori, S., 2003, MNRAS, 344, L13

Ettori, S. & Fabian, A. C., 1999, MNRAS, 305, 834

Evrard, A. E., 1997, MNRAS, 292, 289

Fabian, A. C., 1994, ARAA, 32, 277

Fabian, A. C., Nulsen, P. E. J., 1977, MNRAS, 180, 479

Fabian, A. C., Sanders, J. S., Allen, S. W., et al., 2003, MNRAS, 344, L43

Forman, W., Nulsen, P., Heinz, S., et al. 2003, ApJ

Girardi, M., Fadda, D., Escalera, E., Giuricin, G., Mardirossian, F., Mezzetti, M., 1997, ApJ, 490, 56

Inogamov, N. A. & Sunyaev, R. A., 2003, AstL, 29, 791

King, L. J., Clowe, D. I., Schneider, P., 2002, A&A, 383, 60

Kolmogorov, A. N., 1941, Dokl. Akad. Nauk. SSSR, 30, 301

Loeb, A., Mao, S., 1995, Proceedings of the conference *Dark Matter*, University of Maryland, College Park, 1994, S.S. Holt & C.L. Bennett. (eds), American Inst. of Physics Conference Proceedings, Vol. 336, p.330

Markevitch, M., Forman, W. R., Sarazin, C. L., Vikhlinin, A., 1998, ApJ, 503,77

Markevitch, M., Gonzalez, A. H., David, L., Vikhlinin, A., Murray, S., Forman, W., Jones, C., Tucker, W., 2002, ApJ, 567, L27

Matsushita, K., Belsole, E., Finoguenov, A., Böhringer, H., 2002, A&A, 386, 77

Matsushita, K., Finoguenov, A., Böhringer, H., 2003, A&A, 401, 443

McNamara, B. R., Wise, M., Nulsen, P. E. J., et al., 2000, ApJ, 534, 135

Mellier, Y., 1999, ARA&A, 37, 127

Mohr, J. J., Mathiesen, B., Evrard, A. E., 1999, ApJ, 517, 627

Moore, B., Quinn, T., Governato, F., Stadel, J., Lake, G., 1999, MNRAS, 310, 1147

Navarro, J. F., Frenk, C. S., White, S. D. M., 1996, ApJ, 462, 563

Oboukhov, A. M., 1941, Dokl. Akad. Nauk. SSSR, 32, 22

Peterson, J. R., Paerels, F. B. S., Kaastra, J. S., et al., 2001, A&A, 365, 104

Pierre, M., Le Borgne, J. F., Soucail, G., Kneib, J. P., 1996, A&A, 311,413

Pratt, G. W. & Arnaud, M., 2002, A&A, 394, 375

Pratt, G. W., Böhringer, H., Finoguenov, A., 2004, A&A submitted

Schuecker, P., Böhringer, H., Guzzo, L., Collins, C. A., et al., 2001, A&A, 368, 86

Schuecker, P., Guzzo, L., Collins, C. A., Böhringer, H., 2002, 335, 807

Schuecker, P., Finoguenov, A., Miniati, F., Böhringer, H., Briel, U. G., 2004, A&A, 426, 387

Soucail, G., Ota, N., Böhringer, H., Czoske, O., Hattori, M., Mellier, Y., 2000, A&A, 355, 433

Squires, G., Kaiser, N., Fahlman, G., Babul, A., Woods, D., 1996, ApJ, 469, 73

Spergel, D. N., Verde, L., Peiris, H. V., et al. , 2003, ApJS, 148, 175

Vikhlinin, A., Markevitch, M., Murray, S. S., 2002, ApJ, 549, 160

Vogt, C. & Enßlin, T. A., 2003, A&A, 412, 373

Voit, M., 2004, astro-ph/0410173

Wu, Y.-P., 2000, MNRAS, 316, 299

Xue, Y.-J., Böhringer, H., Matsushita, K, 2004, A&A, 420, 833

Zhang, Y.-Y., Böhringer, H., Mellier, Y., Soucail, G., Forman, W., 2004, astro-ph/0408545

Zwicky, F., 1937, ApJ, 86, 217